The Synthesis, Structure and Physical Properties of the Layered Ruthenocuprates $RuSr_2GdCu_2O_8$ and $Pb_2Sr_2Cu_2RuO_8Cl$

Abbie C. Mclaughlin and J. Paul Attfield

Department of Chemistry, University of Cambridge, Lensfield Road, Cambridge CB2 1EW and Interdisciplinary Research Centre in Superconductivity, Department of Physics, University of Cambridge, Madingley Road, Cambridge CB3 0HE, UK.

Abstract. Studies of the structure and physical properties of the layered ruthenocuprates $RuSr_2GdCu_2O_8$ and $Pb_2Sr_2Cu_2RuO_8Cl$ are reviewed. $RuSr_2GdCu_2O_8$ is a weak ferromagnetic superconductor and doping studies have shown that it is possible to tune the magnetic and superconducting transitions simultaneously. The average crystal structure of $RuSr_2GdCu_2O_8$ is tetragonal at both 10 and 295 K (space group $P4/mmm$), but a $\sqrt{2}a$ x $\sqrt{2}a$ x c superstructure resulting from coherent rotations of the RuO_6 octahedra within subdomains of 50-200 Å is observed by selected area electron diffraction (SAED). The same tilts and rotations of the RuO_6 octahedra are observed in semiconducting $Pb_2Sr_2Cu_2RuO_8Cl$, which has strikingly similar magnetic properties to $RuSr_2GdCu_2O_8$. Antiferromagnetic order is observed in the 10 K neutron diffraction pattern with a Ru moment of 1.1(1) μ_B, but a spin-flop transition is observed above a field of 0.5 T.

1 Introduction

The (ferro)magnetic superconductor $RuSr_2GdCu_2O_8$ [1-21] (Fig. 1) is an extremely interesting material, with a maximum T_c = 37 K and T_M = 136 K, where T_c is the superconducting temperature and T_M is the Curie temperature. The superconductivity occurs in the CuO_2 layers and the ferromagnetism arises in the RuO_2 layers. μSR studies have demonstrated that the material is microscopically uniform with no evidence of spatial phase separation of the superconducting and magnetic regions [4]. Initial SQUID magnetometry results showed that the magnetic order in the ruthenate planes was predominantly ferromagnetic and this persists through the onset of superconductivity at 37 K to the lowest temperatures investigated (1.9 K) [1]. Variable field measurements of $RuSr_2GdCu_2O_8$ showed hysteresis with a remanent moment of 0.12 μ_B indicative of a ferromagnetic component in zero field. However G-type antiferromagnetic order within the RuO_2 planes was subsequently observed from neutron scattering [10] experiments. In this model the Ru spins are aligned antiparallel to their neighbours in the ab plane and along c resulting in a doubling of the unit cell in all three directions. The direction of the spins in this model is parallel to the tetragonal c axis. An upper limit of 0.1 μ_B was obtained for the ferromagnetic component, which appears to contradict results from SQUID magnetometry and electronic paramagnetic resonance experiments [18].

Variable field neutron diffraction studies of $RuSr_2GdCu_2O_8$ showed that the Ru spins cant into a ferromagnetic arrangement upon the application of a magnetic field and at 7 T the Ru spins are fully ferromagnetically ordered. Gd^{3+} is paramagnetic down to 2.5 K and orders with the G-type antiferromagnetic structure below this temperature [10]. It is difficult to perform neutron diffraction experiments on $RuSr_2GdCu_2O_8$ because Gd has an extremely high absorption cross section for thermal neutrons and isotopic enrichment with ^{160}Gd is necessary. Only two antiferromagnetic diffraction peaks have been observed in studies to date [10,19] and it is therefore difficult to know whether the Ru spins are canted in the ground state.

$RuSr_2YCu_2O_8$ has recently been synthesised under a pressure of 5.5 GPa [22]. It is superconducting at $T_c \geq 25$ K and appears to be ferromagnetic, T_M = 149 K, from SQUID magnetometry experiments. Neutron diffraction on this material has also evidenced antiferromagnetic order with a G-type structure and an increased intensity on the [001] peak giving an estimate for the ferromagnetic moment of 0.3 μ_B. Only the $[\frac{1}{2}\frac{1}{2}\frac{1}{2}]$ magnetic diffraction peak was observed from neutron diffraction on $RuSr_2YCu_2O_8$ due to the low signal to noise ratio and so it is still impossible to know whether the spins are canted in the ground state. However the observation of a ferromagnetic component on the [001] peak at ~145 K which is equivalent to 0.3 μ_B at 10 K gives increasing evidence of this. Upon application of a magnetic field the intensity of the antiferromagnetic $[\frac{1}{2}\frac{1}{2}\frac{1}{2}]$ peak decreases and the magnetic structure becomes increasingly ferromagnetic as for $RuSr_2GdCu_2O_8$ [10]. Hence it appears that coexisting super-
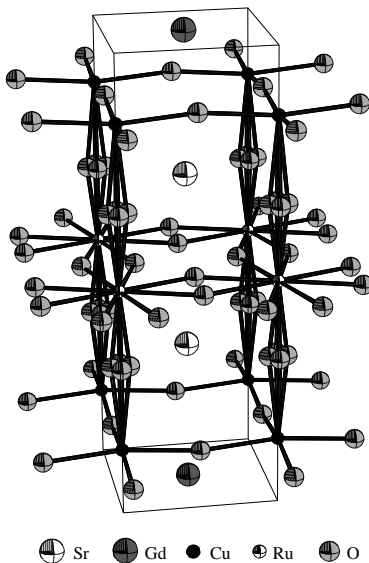

Sr   Gd   Cu   Ru   O

Fig. 1. The average crystal structure of $RuSr_2GdCu_2O_8$ showing the disordered rotations and tilts of the RuO_6 octahedra.

conductivity and weak ferromagnetism occurs in these ruthenocuprates with a transition to full ferromagnetism at high fields. Coexisting ferromagnetism and superconductivity have also been observed in the 1222-type ruthenocuprates $RuSr_2RE_{2-x}Ce_xCu_2O_{10}$ [1,2] RE = Eu, Gd. So far no evidence of antiferromagnetism has been observed from neutron diffraction experiments on these materials [23] and SQUID magnetometry experiments on $RuSr_2EuCeCu_2O_{10}$ have indicated a sizeable ferromagnetic component.

In this paper our studies of the structural and physical properties of $RuSr_2GdCu_2O_8$ will be reviewed. A new phase $Pb_2Sr_2Cu_2RuO_8Cl$ which has strikingly similar magnetic properties to $RuSr_2GdCu_2O_8$ has recently been synthesised [24] and its basic structural and physical properties are discussed within.

2   The Structure and Microstructure of $RuSr_2GdCu_2O_8$

The physical properties of $RuSr_2GdCu_2O_8$ are strongly dependent on the preparation conditions [1]. An "as prepared" sample [5] synthesised by heating in flowing oxygen for 10 hours at 1050 °C and 1055 °C has $T_c \geq 21$ K. However annealing the same sample for 7 days in flowing oxygen at 1050 °C increases T_c to 37 K and halves the 300 K resistivity. We have shown that this occurs due to features of the structure and microstructure of $RuSr_2GdCu_2O_8$. $RuSr_2GdCu_2O_8$ has a tetragonal unit cell at all temperatures [5,6] (space group $P4/mmm$, $a =$ 3.83955(1), $c = 11.57239(7)$ Å) and is cation and oxygen stoichiometric (Fig. 1). Thermogravimetric analysis performed on the annealed sample gave an oxygen stoichiometry of 7.99 ± 0.03. Disorder of the oxygen atoms in the ruthenate planes and the apical atoms linking the CuO_5 units and the RuO_6 octahedra have been observed from synchrotron X-ray diffraction measurements. The in-plane Ru-O bond length (1.969(2) Å) is larger than the in-plane Cu-O bond length (1.9268(4) Å) at 295 K and it is this bond mismatch which results in rotations of the RuO_6 octahedra around the c axis, by 13° at 295 K, with a net stabilisation of the structure. There is also a slight tilting of the octahedra, which reduces the Cu-O-Ru angle to $\sim 173°$. The thermal contraction of the in-plane Cu-O bond is greater than that of the Ru-O bond distances and therefore results in an increase of the bond mismatch between the two bond lengths. This has the effect of rotating the RuO_6 octahedra around c with a slightly increasing angle as the temperature decreases. Hence the displacement of the oxygen atoms actually increases with decreasing temperature proving that they are due to static disorder within the average structure.

The rotations of the RuO_6 octahedra around c that are observed from synchrotron X-ray diffraction on $RuSr_2GdCu_2O_8$ would give rise to a $\sqrt{2}a$ x $\sqrt{2}a$ x c superstructure if long-range ordered. This superstructure was observed in SAED patterns for the "as prepared" $RuSr_2GdCu_2O_8$ sample viewed down the [001] axis (Fig. 2) [5]. All of the main diffraction spots in the SAED pattern could be indexed by the basic tetragonal unit cell and the additional weak spots indicated the formation of a $\sqrt{2}a$ x $\sqrt{2}a$ x c supercell. However there was no evidence for this supercell from synchrotron X-ray diffraction measurements
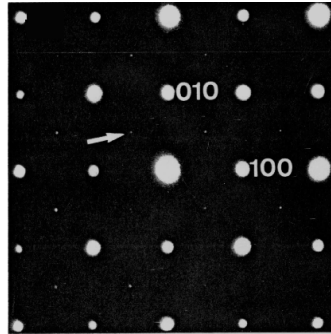
Fig. 2. The SAED pattern from the as prepared $RuSr_2GdCu_2O_8$ sample viewed down the [001] direction. The additional weak spots arrowed evidence the $\sqrt{2}a$ x $\sqrt{2}a$ x c superstructure.

[5,6] which have an extremely high sensitivity to weak diffraction peaks. A High Resolution Transmission Electron Microscopy (HRTEM) image for the annealed $RuSr_2GdCu_2O_8$ sample shows dark rectangular boundaries which divide the structure into sub-domains of 50-200 Å (Fig. 3). It was concluded that there is no long range order of the RuO_6 octahedra and the ordering of the RuO_6 octahedra over many unit cells is shown in Fig. 4. Anti-phase boundaries of width a occur every 50-200 Å as seen in the HRTEM image. At an anti-phase boundary the sense of rotation of the RuO_6 octahedra is reversed, but the remainder of the structure is unaffected. This therefore explains why the electron diffraction but not the X-ray diffraction sees the superstructure, because 50-200 Å is too short to give rise to superstructure peaks in the X-ray data.
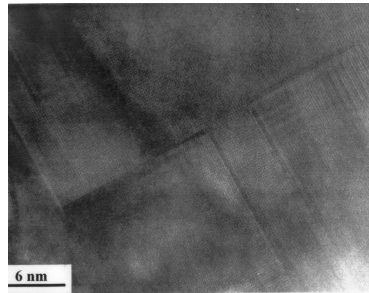

Fig. 3. HRTEM image of the annealed $RuSr_2GdCu_2O_8$ sample viewed down the [001] zone axis showing rectangular anti-phase boundaries.

The c/a axis ratio for $RuSr_2GdCu_2O_8$ at 3.015 (295 K) is very close to ideal for a triple perovskite, for comparison c/a varies between 3.032 and 3.066 as δ

varies from 0 to 1 in YBa$_2$Cu$_3$O$_{7-\delta}$ [25]. The near coincidence of a and b with $c/3$ in RuSr$_2$GdCu$_2$O$_8$ results in the formation of many small domains with c in one of the three equivalent directions as shown in the HRTEM image for the "as prepared" RuSr$_2$GdCu$_2$O$_8$ sample (Fig. 5). The areas labelled A, B, and C are individual domains. The 90° angle between the CuO$_2$ planes meeting at the boundaries strongly reduces the supercurrent transport leading to high granularity, a low transport T$_c$ and a high residual resistivity in the "as prepared" sample. The microstructure of RuSr$_2$GdCu$_2$O$_8$ therefore depends on the synthesis and annealing time; when annealing the sample in oxygen at high temperature for a long time, the improvement in the superconducting properties is due to an increase in domain size, rather than a change in cation composition or oxygen content. This was later confirmed by heat capacity studies which showed that the thermodynamic critical temperature occurs at 46 K in both samples [9].
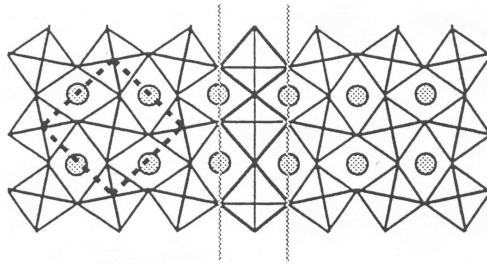

Fig. 4. A model for the rotations of the RuO$_6$ octahedra around c in the RuSr$_2$GdCu$_2$O$_8$ structure, resulting in the $\sqrt{2}a$ x $\sqrt{2}a$ x c superstructure shown in the xy plane by broken lines. An anti-phase boundary is also shown.

No large changes in any of the bond lengths or angles have been observed by powder X-ray diffraction when the Ru moments order at 132 K [6]. The atomic displacement U-factor for the in-plane O(2) changes from 0.009 to 0.011 Å^2 and is the only observed structural anomaly accompanying the magnetic ordering transition. However a variable temperature powder neutron diffraction study of a ^{160}Gd-substituted RuSr$_2$GdCu$_2$O$_8$ sample observed abrupt changes in the Cu-O(2)-Cu buckling angle and the Cu-Cu interlayer distance at T$_M$ [11] and hence the anomaly in the U-factor of O(2) suggests that similar structural changes occur over a shorter range.

The observation of this anomaly at T$_M$ in the CuO$_2$ planes rather than in the RuO$_6$ octahedra is surprising but correlates with magnetoresistance measurements performed on RuSr$_2$GdCu$_2$O$_8$ [26] which show a strong exchange interaction (J = 35 meV) between the spins and the carriers comparable to the superconducting energy gap. It was concluded that the carriers are associated with both CuO$_2$ and RuO$_2$ bands i.e. itinerant electron ferromagnetism because suppression of superconductivity due to exchange is expected if the carriers are

only on the CuO_2 planes. Therefore if the Ru moments are itinerant then this could cause anomalies due to magnetic ordering to manifest in the CuO_2 planes rather than in the RuO_6 octahedra as observed in the synchrotron X-ray [5] and neutron diffraction [11] data. However this contradicts the recent observation of antiferromagnetic order in the ruthenate planes from a different neutron diffraction study [10].
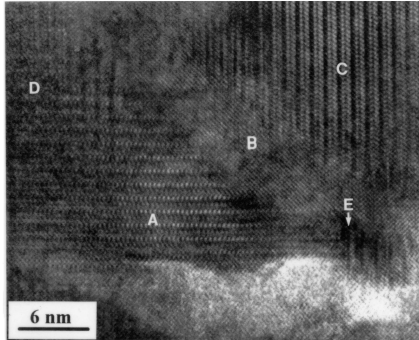

Fig. 5. HRTEM image of a regions of the "as prepared" $RuSr_2GdCu_2O_8$ sample showing the multi-domain nature of the microstructure. The areas labelled A, B, and C are individual domains. A and C are both orientated in the [100] direction, but rotated by 90° from one another whilst domain B ([001] orientation) is perfectly intergrown between A and C without any amorphous boundaries. Area D shows an intergrowth of A and B with an interface on the [100] plane for both domains. The intergrowth of A and B in the area E is between the [010] plane of A and the [001] plane of B.

$RuSr_2GdCu_2O_8$ is thought to be a canted antiferromagnet (a weak ferromagnet). The slight canting of the Ru moments can arise due to a Dzyaloshinsky-Moriya [27,28] interaction (antisymmetric exchange interaction between neighbouring Ru moments) which is non-zero due to the tilts and rotations of the RuO_6 octahedra. Previous transport measurements on $RuSr_2GdCu_2O_8$ indicated a hole concentration on the CuO_2 planes of $p = 0.07$ [1]. Bond valence summations [29] on $RuSr_2GdCu_2O_8$ resulted in a large estimation of the hole concentration in the cuprate planes; $p = 0.44$. The canting of the Ru moments due to the Dzyaloshinsky-Moriya interaction could lead to magnetic trapping or scattering of the holes and hence transport properties typical of underdoped cuprates, whilst the apparent hole concentration measured crystallographically is much higher. However Brown et al [30] have shown that bond valence sum calculations do not give accurate results if the bond lengths are strained. The Cu-O bonds are strained in $RuSr_2GdCu_2O_8$ due to the bond mismatch between the ruthenate and cuprate layers which could therefore explain the discrepancy in the two estimations of p from transport measurements and bond valence sums.

3   Doping Studies of $RuSr_2GdCu_2O_8$

The substitution of Ru by the non-magnetic, fixed valent cations Nb^{5+} and Sn^{4+} has helped in the understanding of the charge distribution and magnetism of $RuSr_2GdCu_2O_8$. The hole doping of the copper oxide planes necessary to induce superconductivity arises from the overlap of the minority spin Ru: t_{2g} and the Cu: $3d_{x^2-y^2}$ bands and the formula is written as $Ru^{5-2p_0}Sr_2Gd(Cu^{2+p_0})_2O_8$ to show the average Ru and Cu oxidation states [31,32].

The $Ru_{1-x}M_xSr_2GdCu_2O_8$ solid solutions have been studied by powder X-ray diffraction [31,32] and the observation of overall increases in the lattice parameters, cell volume, Sr-O and Ru/M-O bond lengths are in accordance with the substitution of the slightly larger Sn^{4+} and Nb^{5+} for $Ru^{4+}/^{5+}$. The RuO_6 octahedra were found to rotate around c with a greater angle as x increases in the $Ru_{1-x}M_xSr_2GdCu_2O_8$ solid solutions due to the increased bond mismatch between the in plane Ru-O and Cu-O bonds. An increase in the average apical Cu-O bond was also observed with Nb substitution due to the change in charge transfer from the minority spin Ru: t_{2g} to the Cu: $3d_{x^2-y^2}$ bands [31,32]. Similar results were found upon reduction of $YBa_2Cu_3O_7$ [25] in which the apical bond increases from 2.328(3) Å to 2.380(4) Å and the T_c decreases from 69 to 56 K.
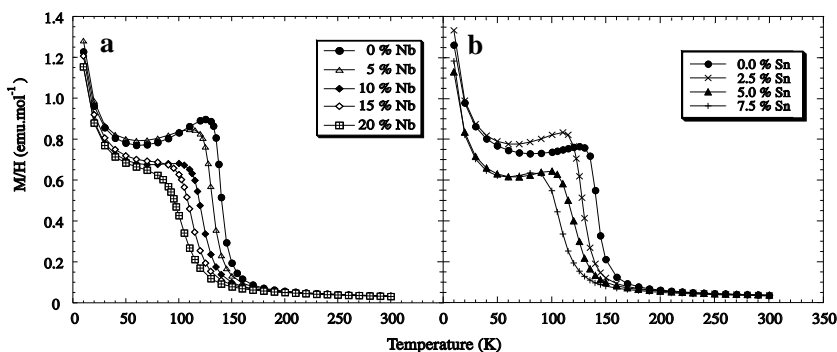

Fig. 6. Variation of molar susceptibility with x in (**a**) the $Ru_{1-x}Nb_xSr_2GdCu_2O_8$ solid solutions and (**b**) $Ru_{1-x}Sn_xSr_2GdCu_2O_8$ solid solutions.

The magnetic properties of $RuSr_2GdCu_2O_8$ were found to change dramatically with Sn/Nb substitution for Ru. Magnetic hysteresis loops recorded at 10 K confirmed the ferromagnetic order in all samples. A reduction of the Curie temperature (T_M) and a broadening of the magnetic transition were clearly observed with both Sn and Nb substitution (Fig. 6). The Ru moment, remanent moment and coercive field measured for all samples were also found to decrease smoothly with x in the $Ru_{1-x}M_xSr_2GdCu_2O_8$ solid solutions. The fixed valent diamagnetic cations do not contribute electronic states close to the Fermi level and therefore the substitution of diamagnetic Sn^{4+} and Nb^{5+} dilutes the ferromagnetism in the RuO_2 layers leading to a rapid decrease in the Curie temperature

from 136 K to 103 K in $Ru_{0.8}Nb_{0.2}Sr_2GdCu_2O_8$. The estimated moment per Ru atom decreases with x due to the disorder of the spins incurred by substitution of the non-magnetic cations.
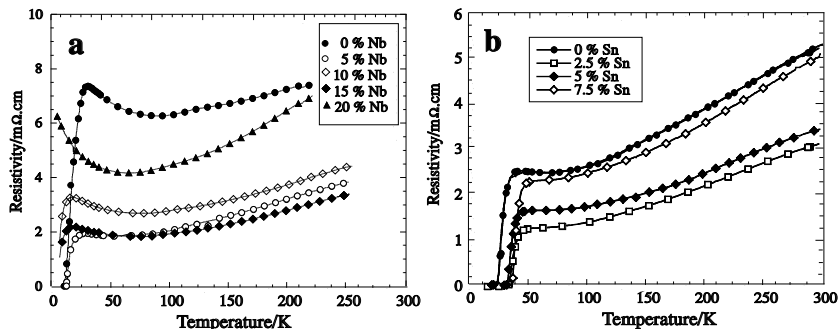

Fig. 7. Variation of the resistivity with x for **(a)** the $Ru_{1-x}Nb_xSr_2GdCu_2O_8$ solid solutions and **(b)** the $Ru_{1-x}Sn_xSr_2GdCu_2O_8$ solid solutions.

Superconducting transitions were observed for the $Ru_{1-x}Nb_xSr_2GdCu_2O_8$ solid solutions with $x = 0$ - 0.15 (Fig. 7(**a**)) but not for $x = 0.2$ down to 7 K. All the $Ru_{1-x}Sn_xSr_2GdCu_2O_8$ samples were superconducting (Fig. 7(**b**)) and the onset T_c was found to increase from 38 K for $RuSr_2GdCu_2O_8$ to 50 K in the 7.5 % Sn sample. All samples were observed to be metallic ($d\rho/dT > 0$) although a semiconducting upturn was observed close to T_c. Therefore substitution of $Ru^{4.84+}$ by Nb^{5+} leads to the removal of holes from the CuO_2 planes so that the materials become more underdoped. This is supported by the increase in the 290 K Seebeck coefficient with x in the $Ru_{1-x}Nb_xSr_2GdCu_2O_8$ solid solutions [31,32] and the decrease in T_c to 19 K in the 15 % Nb sample. The opposite effect occurs upon Sn substitution; the hole concentration increases with a subsequent increase in T_c to 50 K and a decrease in the Seebeck coefficient (Fig. 8). Thermogravimetric analysis on the $Ru_{1-x}M_xSr_2GdCu_2O_8$ solid solutions showed that there is no change in oxygen content with increasing Nb^{5+}/Sn^{4+} substitution. The charge distribution in the doped ruthenocuprates was therefore written as $(Ru^{5-2p_0})_{1-x}M^q_xSr_2Gd(Cu^{2+p_0+\Delta p})_2O_8$ where the extrinsic doping introduced by the substituents M of charge q is $\Delta p = (5 - q - 2p_0)x/2$, assuming the initial doping level p_0 remains constant. The fitted value of p_0 is 0.08.

The maximum T_c for $RuSr_2GdCu_2O_8$ has been estimated at 65(10) K by fitting the values of the T_c onset measured for the $Ru_{1-x}M_xSr_2GdCu_2O_8$ solid solutions to the quadratic equation $T_c = T_c^{max}[1 - 82.6(p - 0.16)^2]$ [33] (Fig. 9). This is in agreement with the $T_c^{max} = 72$ K recently recorded for $Ru_{1-x}Sr_2GdCu_{2+x}O_{8-y}$ at optimal doping [34]. This is much lower than the highest T_c of 105 K obtained for the 1212 cuprate $(Tl_{0.5}Pb_{0.5})Sr_2(Ca, Y)Cu_2O_7$ [35]. It was speculated that this suppression could reflect a pairbreaking interaction with the ferromagnetic moments in the RuO_2 plane. However this effect would be ex-
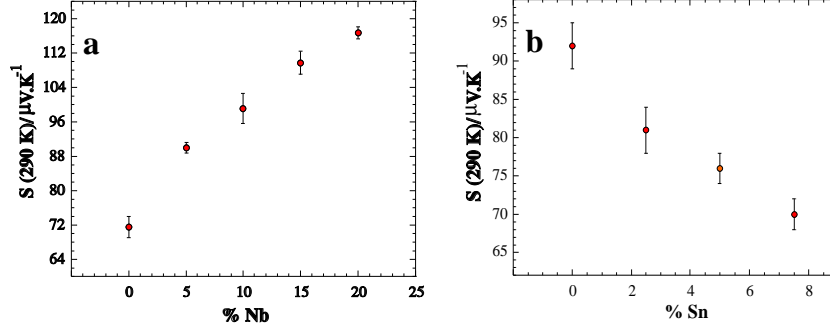
Fig. 8. Variation of the room temperature Seebeck coefficient with x for **(a)** the Ru$_{1-x}$Nb$_x$Sr$_2$GdCu$_2$O$_8$ solid solutions and **(b)** the Ru$_{1-x}$Sn$_x$Sr$_2$GdCu$_2$O$_8$ solid solutions.
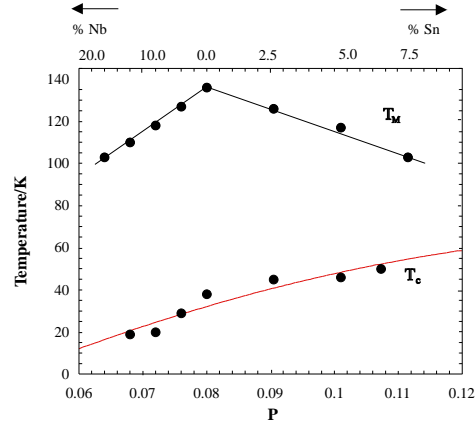

Fig. 9. The variation of the superconducting critical temperature (T$_c$) and the Curie temperature (T$_M$) with doping level p (lower scale) and % Nb or Sn (upper scale) in the Ru$_{1-x}$M$_x$Sr$_2$GdCu$_2$O$_8$ solid solutions. The T$_c$ values are fitted by the quadratic expression supplied in the text.

pected to be greater in the undoped compound and it was concluded that the low estimate of T$_c^{max}$ is due to the lattice strain from the bond mismatch between the cuprate and ruthenate layers which increases upon substitution of both Sn and Nb. The unusually short apical Cu-O bond of 2.16 Å in RuSr$_2$GdCu$_2$O$_8$ provides evidence that the geometry of this tetragonal 1212 structure is not optimal for superconductivity. As a consequence bond valence sums give $p \sim 0.4$ for RuSr$_2$GdCu$_2$O$_8$ whereas results from transport measurements led to an estimate of $p \sim 0.1$. It was originally thought that this discrepancy was due to a large number of holes trapped by defects or by the ferromagnetic order in the sample. However upon dilution of the weak ferromagnetism there was no evidence of a disproportionately large increase in p from the room temperature Seebeck coef-

ficient or the transport properties of the $Ru_{1-x}M_xSr_2GdCu_2O_8$ samples. Earlier results on $YBa_2Cu_3O_{7-\delta}$ [30] have shown that bond valence sum calculations do not work well on structures under strain. The structure of $RuSr_2GdCu_2O_8$ is strained due to the bond mismatch between the ruthenate and cuprate layers and it is therefore concluded that the actual hole concentration in the cuprate planes is $p \sim 0.08$ and that there are no additional, magnetically trapped holes.

4   The Structure and Magnetic Properties of $Pb_2Sr_2Cu_2RuO_8Cl$

A new material $Pb_2Sr_2Cu_2RuO_8Cl$ (Fig. 10) has recently been synthesised [24] enabling further study of the electronic and magnetic properties of the rutheno-cuprates. This material is of similar structure to $RuSr_2GdCu_2O_8$ but caesium chloride type Pb_2Cl layers replace Gd making the material more convenient to study by neutron diffraction. Such a CsCl-type Pb_2Cl layer also exists in the mineral ferrate $Pb_4Fe_3O_8Cl$ known as hematophanite [36,37] and the isostructural insulating materials $Pb_2Sr_2Cu_2MO_8Cl$ (M = Ta, Nb, Sb) [38 - 40].

   $Pb_2Sr_2Cu_2RuO_8Cl$ has been studied by TOF neutron diffraction between 295 and 10 K [24]. This phase is difficult to prepare free of secondary phases and the sample contained 73 % $Pb_2Sr_2Cu_2RuO_8Cl$ by mass with 8 % CuO and 19 % "SrRuO$_3$". An excellent Rietveld fit was obtained at all temperatures with a tetragonal $P4/mmm$ symmetry structural model for the principal phase (a = 3.86681(9) Å, c = 15.3688(7) Å at 295 K). The oxygen atoms within the
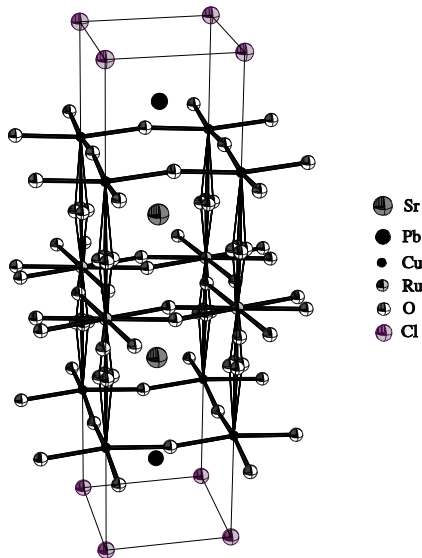

Fig. 10. The average crystal structure of $Pb_2Sr_2Cu_2RuO_8Cl$ showing the tilts and rotations of the RuO_6 octahedra.

RuO_6 planes and the oxygen atoms linking the CuO_5 units and RuO_6 octahedra (Fig. 10) were found to be disordered as observed for $RuSr_2GdCu_2O_8$ [5,6]; the RuO_6 octahedra are rotated by 13.4° around the z axis and are tilted away from this axis by 7.1° at room temperature. A recent BVS calculation on $Pb_2Sr_2Cu_2RuO_8Cl$ has shown that the hole transfer to the CuO_2 planes is ~0.1 less than in $RuSr_2GdCu_2O_8$; the apical Cu-O distance (2.24 Å) is longer than that in $RuSr_2GdCu_2O_8$ (2.16 Å) at room temperature. Hence since p was estimated at 0.08 in $RuSr_2GdCu_2O_8$ it was concluded that the CuO_2 planes in $Pb_2Sr_2Cu_2RuO_8Cl$ are essentially undoped. $Pb_2Sr_2Cu_2RuO_8Cl$ is semiconducting with a room temperature resistivity of 160 Ω.cm and there is no evidence for a superconducting transition at low temperatures, consistent with the copper oxide planes being too underdoped to superconduct.
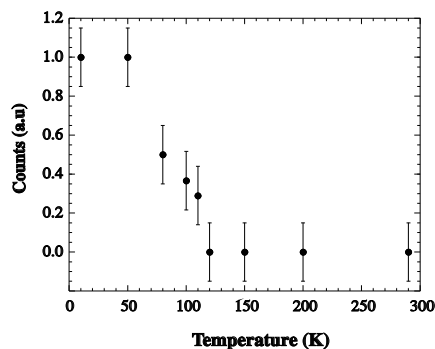

Fig. 11. Temperature dependence of the intensity of the magnetic $[\frac{1}{2}\frac{1}{2}\frac{1}{2}]$ neutron diffraction peak.

A variable temperature neutron study has shown that $Pb_2Sr_2Cu_2RuO_8Cl$ appears to be antiferromagnetic below 120 K as the $[\frac{1}{2}\frac{1}{2}\frac{1}{2}]$ magnetic diffraction peak is observed below this temperature (Figs. 11 and 12). The low temperature neutron diffraction patterns were fitted with the same G-type antiferromagnetic model as for $RuSr_2GdCu_2O_8$ [10]. The spins were assumed to lie parallel to the c axis giving a refined Ru moment of 1.1(1) μ_B. This value is within error of the value $\mu_{Ru} = 1.18(6)$ μ_B in $RuSr_2GdCu_2O_8$ [10]. There was no observation of a change in the nuclear Bragg intensity of any of the $[00l]$ peaks where the ferromagnetic contribution would be expected between 295 K and 10 K. A variable field neutron diffraction study has recently been performed on $Pb_2Sr_2Cu_2RuO_8Cl$ [41]. These measurements have shown that at fields higher than 0.5 T the intensity of the $[\frac{1}{2}\frac{1}{2}\frac{1}{2}]$ magnetic peak decreases whilst an increase of the $[003]$ peak intensity is observed corresponding to induced ferromagnetism in the xy plane (Fig.13). No significant $[\frac{1}{2}\frac{1}{2}\frac{1}{2}]$ intensity was observed above 1.1 T and the effect of the magnetic field was found to be reversible; returning to zero field, the $[\frac{1}{2}\frac{1}{2}\frac{1}{2}]$ peak recovers its original intensity. Evidence of such a spin-flop transition has previously been reported in $RuSr_2GdCu_2O_8$ at 0.4 T [8] and

$RuSr_2YCu_2O_8$ [22]. It was concluded that the field dependent magnetic order is common to the ruthenocuprate structures but further neutron diffraction experiments on a phase pure $Pb_2Sr_2Cu_2RuO_8Cl$ sample will be necessary in order to confirm this.
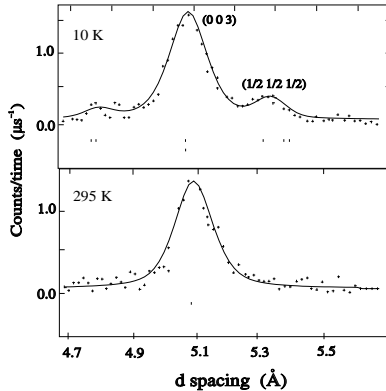

Fig. 12. Part of the neutron diffraction pattern of $Pb_2Sr_2Cu_2RuO_8Cl$ showing the weak nuclear [003] peak along with the $[\frac{1}{2}\frac{1}{2}\frac{1}{2}]$ antiferromagnetic Bragg peak at 10 K. The same portion at 290 K is shown below for reference.
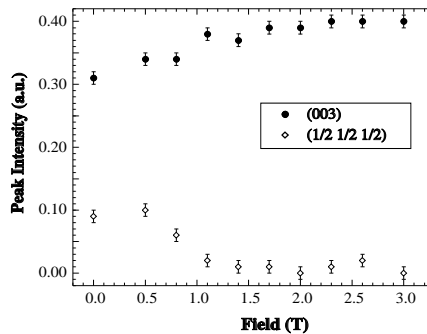

Fig. 13. Field dependence of the intensity of the magnetic $[\frac{1}{2}\frac{1}{2}\frac{1}{2}]$ and nuclear [003] neutron diffraction peaks.

A ferromagnetic transition at $T_M = 117(1)$ K was evidenced from SQUID magnetometry measurements on $Pb_2Sr_2Cu_2RuO_8Cl$ (Fig. 14) despite the observation of antiferromagnetism in the variable temperature neutron diffraction study. Similar SQUID magnetometry results were observed for $RuSr_2GdCu_2O_8$ [1]. No separate ferromagnetic transition was observed for the "$SrRuO_3$" secondary phase showing that substitutions by Pb or Cu have suppressed the
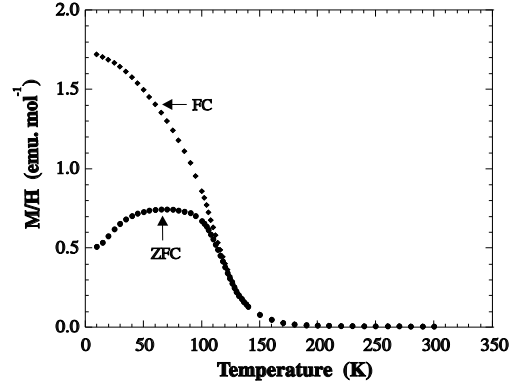
Fig. 14. Variable temperature molar susceptibility for Pb$_2$Sr$_2$Cu$_2$RuO$_8$Cl.

ferromagnetism found in pure SrRuO$_3$ (T$_M$ = 165 K); a suppression of the ferromagnetic state in the SrRu$_{1-x}$Pb$_x$O$_3$ system [42] has been reported previously. Furthermore there was no observable ferromagnetic contribution from the "SrRuO$_3$" phase in the 10 K neutron pattern. Magnetic hysteresis loops recorded at 10 K (Fig. 15) yielded a moment of 0.8(1) μ_B per Ru atom. The presence of 19% SrRuO$_3$ which has a μ_{Ru} = 1.4 μ_B at 5 T [42] could only contribute ∼0.3 μ_B to the sample magnetisation per Ru, even if it were stoichiometric. Hence it was concluded that the saturated Ru moment in Pb$_2$Sr$_2$Cu$_2$RuO$_8$Cl is 0.5 - 0.8 μ_B which is comparable to the value of 1.09 μ_B in RuSr$_2$GdCu$_2$O$_8$ [31,32]. A narrowing of the hysteresis loop for Pb$_2$Sr$_2$Cu$_2$RuO$_8$Cl was observed at low fields, indicative of a spin flop transition from weak ferromagnetism to full ferromagnetism above 0.5 T consistent with the variable field neutron diffraction results. It was therefore concluded that Pb$_2$Sr$_2$Cu$_2$RuO$_8$Cl is a canted antifer-
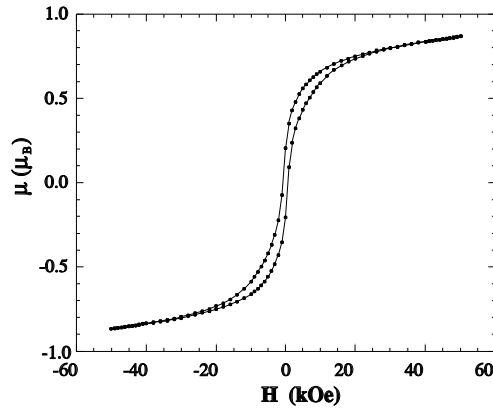
Fig. 15. Variable field magnetisation data for the Pb$_2$Sr$_2$Cu$_2$RuO$_8$Cl sample.

romagnet with an ordered moment of 1.1 μ_B per Ru in zero field below $T_M = $ 117 K. The Ru spins cant into a fully ferromagnetic arrangement above H = 0.5 T giving a saturated Ru moment of 0.5 - 0.8 μ_B.

5   Conclusions

The structures of the (ferro)magnetic superconductor $RuSr_2GdCu_2O_8$ and the new layered ruthenocuprate $Pb_2Sr_2Cu_2RuO_8Cl$ have been studied. There are marked similarities in both the structure and basic magnetic properties of these materials. Both materials contain CuO_5 units separated by RuO_2 planes (Figs. 1 and 10). The RuO_6 octahedra are rotated by approximately 13° in both materials due to a bond mismatch between the in-plane Ru-O and Cu-O bond lengths. Tilts of the RuO_6 octahedra which reduce the Cu-O-Cu angle to ~173° are also observed for both $RuSr_2GdCu_2O_8$ and $Pb_2Sr_2Cu_2RuO_8Cl$. $RuSr_2GdCu_2O_8$ and $Pb_2Sr_2Cu_2RuO_8Cl$ are believed to be canted antiferromagnets in zero field below $T_M = $ 132 K and 117 K respectively. The canting of the Ru moments arises due to a Dzyaloshinsky-Moriya interaction between neighbouring Ru moments which is non-zero due to the tilts and rotations of the RuO_6 octahedra. Upon the application of magnetic field the Ru moments cant into a ferromagnetic arrangement above H = 0.5 T giving a saturated Ru moment of 0.5 - 0.8 μ_B and 1.09 μ_B in $Pb_2Sr_2Cu_2RuO_8Cl$ and $RuSr_2GdCu_2O_8$ respectively. The maximum T_M is plotted against the Ru-Ru interplanar distance for the three ruthenocuprate structure types $RuSr_2GdCu_2O_8$, $RuSr_2Eu_{1.4}Ce_{0.6}Cu_2O_{10}$ [43] and $Pb_2Sr_2Cu_2RuO_8Cl$ in Fig. 16. The inverse correlation shows that T_M is limited by the interplanar superexchange coupling between RuO_2 planes, as expected for these layered magnetic systems.
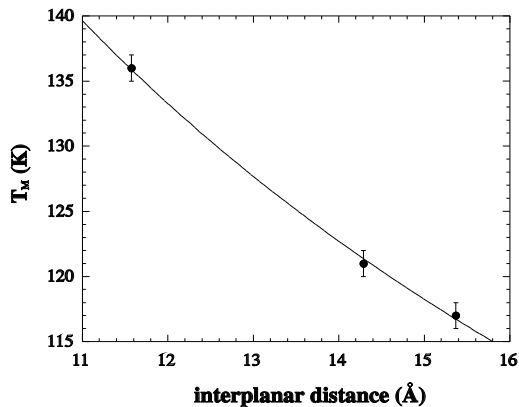

Fig. 16. The variation of T_M with Ru-Ru interplanar distance in ruthenocuprates.

Doping studies of $RuSr_2GdCu_2O_8$ have shown that the overlap of the Cu $3d_{x^2-y^2}$ and the Ru t_{2g} bands leads to the hole doping of the CuO_2 planes re-

quired for superconductivity. A tuning of both the ferromagnetic and superconducting transitions is observed with increasing x in the $Ru_{1-x}M_xSr_2GdCu_2O_8$ solid solutions (M = Nb, Sn). Despite the structural and magnetic similarities of $RuSr_2GdCu_2O_8$ and $Pb_2Sr_2Cu_2RuO_8Cl$, the carrier distribution in $Pb_2Sr_2Cu_2$-RuO_8Cl appears to be different. $RuSr_2GdCu_2O_8$ is superconducting below T_c = 37 K whereas $Pb_2Sr_2Cu_2RuO_8Cl$ is semiconducting and the longer apical Cu-O distance suggests that the CuO_2 planes are essentially undoped. The RuO_2 planes of $Pb_2Sr_2Cu_2RuO_8Cl$ thus contain Ru^{5+} with little or no electron doping to the Ru^{4+} state. This confirms that the weak ferromagnetism in the layered ruthenocuprates arises from the local symmetry breaking distortions rather than a mixed Ru^{4+}/Ru^{5+} state.

Acknowledgements

References

1. J. L. Tallon, C. Bernhard, M. Bowden, P. Gilberd, T. Stoto and D. Pringle: IEEE. Trans. Appl. Supercon. **9**, 1696 (1999)
2. L. Bauernfeind, W. Widder and H. F. Braun: Physica C **254**, 151 (1995)
3. L. Bauernfiend, W. Widder and H. F. Braun: J. Low Temp. Phys. **105**, 1605 (1996)
4. C. Bernhard, J. L. Tallon, C. Niedermayer, T. Blasius, A. Golnik, E. Brucher, R. K. Kremer, D. R. Noakes, C. E. Stronach and E. J. Ansaldo: Phys. Rev. B **59**, 14099 (1999)
5. A. C. Mclaughlin, W. Zhou, J. P. Attfield, A. N. Fitch and J. L. Tallon: Phys. Rev. B **60**, 7512 (1999)
6. A. C. Mclaughlin, J. P. Attfield and J. L. Tallon: Int. J. Inorg. Mater. **2**, 95 (2000)
7. K. B. Tang, Y. T. Qian, L. Yang, Y. D. Zhao and Y. H. Zhang: Physica C **282-287**, 947 (1997)
8. I. Felner, U. Asaf, S. Reich and Y. Tsabba: Physica C **163**, 311 (1999)
9. J. L. Tallon, J. W. Loram, G. V. M. Williams and C. Bernhard: Phys. Rev. B **61**, 6471 (2000)
10. J. W. Lynn, B. Keimer, C. Ulrich, C. Bernhard and J. L. Tallon: Phys. Rev. B **61**, 14964 (2000)
11. O. Chmaissam, J. D. Jorgensen, H. Shaked, P. Dollar and J. L. Tallon: Phys. Rev. B **61**, 6401 (2000)
12. X. H. Chen, Z. Sun, K. Q. Wang, S. Y. Li, Y. M. Xiong, M. Yu and L. Z. Cao: Phys. Rev. B **63**, 54506 (2001)
13. K. Nakamura, K. T. Park, A. J. Freeman and J. D. Jorgensen: Phys. Rev. B **63**, 24507 (2001)
14. Y. Furukawa, S. Takada, A. Yamanaka and K. Kumagai: Physica C **341**, 453 (2000)

15. C. Bernhard, J. L. Tallon, E. Brucher and R. K. Kremer: Phys. Rev. B **61**, 14960 (2000)
16. A. Fainstein, P. Etchegoin, H. J. Trodahl and J. L. Tallon: Phys. Rev. B **61**, 15468 (2000)
17. A. Butera, A. Fainstein, E. Winkler and J. L. Tallon: Phys. Rev. B **63**, 54442 (2001)
18. A. Fainstein, E. Winkler, A. Butera and J. L. Tallon: Phys. Rev. B **60**, 12597 (1999)
19. J. D. Jorgensen, O. Chmaissem, H. Shaked, S. Short, P. W. Klamut, B. Dabrowski, and J. L. Tallon: Phys. Rev. B **63**, 54440 (2001)
20. R. S. Liu, L. Y. Jang, H. H. Hung and J. L. Tallon: Phys. Rev. B **63**, 212507 (2001)
21. A. V. Boris, P. Mandal, C. Bernhard, N. N. Kovaleva, K. Pucher, J. Hemberger and A. Loidl: Phys. Rev. B **63**, 184505 (2001)
22. H. Takagiwa, J. Akimitsu, H. Kawano-Furukawa and H. Yoshizawa: J. Phys. Soc. Jpn. **70**, 333 (2001)
23. C. S. Knee, B. D. Rainford and M. T. Weller: J. Mater. Chem. **10**, 2445 (2000)
24. A. C. Mclaughlin, J. A. McAllister, L. D. Stout and J. P. Attfield: Solid State Sciences, in press (2002)
25. R. J. Cava, A. W. Hewat, E. A. Hewat, B. A. Batlogg, M. Marezio, K. M. Rabe, J. J. Krajewski, W. F. Peck Jr. and L. W. Rupp Jr: Physica C **165**, 419 (1990)
26. J. E. McCrone, J. R. Cooper and J. L. Tallon: J. Low Temp. Phys. **117**, 1199 (1999)
27. I. Dzyaloshinksy: Sov. Phys. JETP **5**, 1259 (1957)
28. T. Moriya: Phys. Rev. **120**, 91 (1960)
29. I. D. Brown: J. Solid State Chem. **82**, 122 (1989)
30. I. D. Brown: J. Solid State Chem. **90**, 155 (1991)
31. A. C. Mclaughlin, V. Janowitz, J. A. McAllister and J. P. Attfield: Chem. Commun. 1331 (2000)
32. A. C. Mclaughlin, V. Janowitz, J. A. McAllister and J. P. Attfield: J. Mater. Chem. **11**, 173 (2001)
33. M. R. Presland, J. L. Tallon, R. G. Buckley, R. S. Liu and N. E. Flower: Physica C **176**, 95 (1991)
34. P. W. Klamut, B. Dabrowski, S. Kolesnik, M. Maxwell and J. Mais: Phys. Rev. B **63**, 224512 (2001)
35. R. S. Liu, P. P. Edwards, Y. T. Huang, S. F. Wu and P. T. Wu: J. Solid State Chem. **86**, 334 (1990)
36. R. C. Rouse: Am. Miner. **56**, 652 (1971)
37. J. Pannetier and P. J. Batail: J. Solid State Chem. **39**, 15 (1981)
38. R. K. Li: Physica C **277**, 252 (1997)
39. R. Li: J. Solid State Chem. **130**, 154 (1997)
40. R. J. Crooks, C. S. Knee and M. T. Weller: Chem. Mater. **10**, 4169 (1998)
41. A. C. Mclaughlin, J. A. McAllister, L. D. Stout and J. P. Attfield: (submitted).
42. G. Cao, S. McCall, J. Bolivar, M. Shepard, F. Freibert, P. Henning and J. E. Crow: Phys. Rev. B **54**, 15144 (1996)
43. I. Felner, U. Asaf, Y. Levi and O. Millo: Phys. Rev. B **55**, 3374 (1997)